Metal Polycation Adduction to Lipids Enables Superior Ion Mobility Separations with Ultrafast Ozone-Induced Dissociation

Alexandre A. Shvartsburg,[1,*] Pawel Sadowski,[2] Berwyck L. J. Poad,[2] Stephen J. Blanksby[2]

1. Department of Chemistry, Wichita State University, 1845 Fairmount, Wichita, KS 67260

2. Central Analytical Research Facility and Faculty of Science, Queensland University of Technology, Brisbane, QLD 4000, Australia

* e-mail: alexandre.shvartsburg@wichita.edu

ABSTRACT: Specific lipid isomers are functionally critical, but their structural rigidity and usually minute geometry differences make separating them harder than other biomolecules. Such separations by ion mobility spectrometry (IMS) were recently enabled by new high-definition methods using dynamic electric fields, but major resolution gains are needed. Another problem of identifying many isomers with no unique fragments in ergodic collision-induced dissociation (CID) was partly addressed by the direct ozone-induced dissociation (OzID) that localizes the double bonds, but low reaction efficiency has limited the sensitivity, dynamic range, throughput, and compatibility with other tools. Typically lipids are analyzed by MS as singly-charged protonated, deprotonated, or ammoniated ions. Here we explore the differential IMS (FAIMS) separations with OzID for exemplary lipids cationized by polyvalent metals. These multiply charged adducts have much greater FAIMS compensation voltages (U_C) than the 1+ ions, with up to 10-fold resolution gain enabling baseline isomer separations even at a moderate resolving power of the Selexion stage. Concomitantly OzID speeds up by many orders of magnitude, producing high yield of diagnostic fragments already in 1 ms. These capabilities can be ported to the superior high-definition FAIMS and high-pressure OzID systems to take lipidomic analyses to the next level.

Lipidomics is a topical area with rapid expansion stimulated by multiple technological advances.[1-3] The liquid chromatography/mass spectrometry (LC/MS) techniques employed in the foundational studies[1,2] are limited by low throughput and insufficient specificity of LC and lack of informative fragments in tandem MS. The latter has been addressed in some cases using three or more consecutive MS steps, at the cost of sensitivity and speed.[1] Full characterization of the isomeric complexity crucial to understand the lipid biochemistry remains a major challenge calling for new methodologies.[4]

Across the application areas (prominently proteomics), the LC and electrophoresis are gradually replaced by fast IMS in gases with unique selectivity.[5] However, linear IMS based on the absolute ion mobility (K) or collision cross section (Ω) at normally moderate electric field (E) is largely parallel to MS because of the correlation between Ω (associated with the physical ion size) and ion mass (m) manifested as the trend lines in IMS/MS palettes.[6-8] This dependence is softened for peptides/proteins by multiple ion charge states z (with distinct trends) and diverse folds (with scatter around those trends),[6] but is tight for lipids with usual z of 1 (or −1) and little conformational flexibility: the mean deviation of K values in representative sets from the trend was 7.3% for 1+ peptides vs. 2.6% for lipids.[8] This impeded linear IMS in lipidomics, wherein broad isomer separation was attained only recently upon reaching the resolving power (R) of ≥200 in the high-pressure drift-tube, trapped, traveling-wave, or cyclic IMS.[9-11]

Another IMS approach of field asymmetric waveform IMS (FAIMS) captures the mobility increment (ΔK) between two E levels.[12,13] The waveform of some amplitude (dispersion voltage, U_D) establishes a field across the gap of width g between two parallel electrodes. This field (with the peak strength $E_D = U_D/g$) deflects the ions pulled along the gap by gas flow toward either electrode at an angle set by ΔK at the E levels in two waveform polarities. A compensation field (E_C) due to U_C on top of the waveform can offset this motion for a species to pass, while others still drift to and are destroyed on the electrodes. Scanning U_C elicits the spectrum of ions entering the gap.

The ion mass or m/z correlate to ΔK much weaker than to K, rendering MS more orthogonal to FAIMS than linear IMS - by (3 - 6)× for typical biomolecules including lipids and peptides.[14,15] Therefore, FAIMS generally resolves isomers better than linear IMS with same R and could distinguish some (including lipids) where best linear IMS stages failed.[10,16] That statistics does not preclude outliers, and linear IMS has outperformed for certain lipid and other isomers.[10,17]

The R metric maximizes in the FAIMS gaps with homogeneous field between planar electrodes, where:[18,19]

$$R = E_C K \sqrt{t_{res}/(D_{II} ln2)}/4 \quad (1)$$

and the ion transmission is:

$$s = \exp(-\pi^2 D_{II} t_{res}/g_e^2) \quad (2)$$

Here, t_{res} is the average ion residence time in the gap (inversely proportional to the gas flow rate Q), D_{II} is the longitudinal diffusion coefficient (comprising the anisotropic terms), and g_e is the effective gap width (equal to g minus the amplitude of ion oscillations in the waveform cycle). Thus the resolution (r) is maximized at longest t, which hinges on wider gaps to prolong the ion survival in free diffusion regime. The buffers with light (He or H_2) and heavier (typically N_2 or CO_2) components often increase R by lifting E_C via the non-Blanc effect.[15-17] Such high-definition (HD) FAIMS devices with g ~ 2 mm and t ~ 100 - 500 ms can reach R ~ 100 for ions with $z = \pm 1$ and up to ~500

for multiply-charged peptides with greater E_C and K values (at equal D_{II}) combining to raise R per eq (1).

The HD-FAIMS can separate sundry isomeric biomolecules including the histone tails,[17] D/L epimers,[15] protein conformers/protomers,[20] and glycoforms. Lipids are routinely ionized via protonation or ammoniation in electrospray ionization (ESI) sources.[4,10,14,16] About 70% of such glycerolipid and phospholipid isomers with swapped fatty acid (FA) chains (transacylation) or positions and/or cis/trans symmetry of double bond (DB) were at least partly resolved.[14] However, the long t and low ion utilization per eq (2) have restricted the sensitivity and necessitated long E_C scans exceeding regular LC peak widths.[16] The FAIMS systems with lower t can be more sensitive and/or permit faster scans, e.g., SelexION (Sciex)[21] with smaller g = 1 mm and shorter planar cell has t ~ 10 ms. However, that limited R for lipids (in N_2 gas) to ~10 and most isomers merged.[22,23]

New avenues in lipidomics were opened by complementing the ergodic MS/MS via CID by direct ultraviolet photodissociation[24,25] and OzID mimicking the ozonolysis in solution.[26-28] The OzID severs DBs but not the weaker single bonds, permitting one to localize the DBs based on the Criegee (C) and Aldehyde (A) fragments differing by an O atom (16 Da). One could thus delineate the DB position isomers in biological matrices, with some cis- and trans- geometries disentangled by the quantitative yields using standards.[27]

In practice, O_3 is doped in the gas pumped to the MS region intended for CID (e.g., the ion trap or collision cell). The competition is tilted toward OzID by higher O_3 partial pressure (P_{O3}), longer dwell time (t_{Oz}), and minimal ion injection energy.[28] Ozone is generated by arc discharge in O_2, providing up to ~20% O_3 (v/v). That and collision gas pressure of ~10^{-5} Torr in ion traps meant low P_{O3} and thus long t_{Oz} (>1 s) even for modest yields. Subsequent implementations in the triple-quadrupole MS instruments (with Q2 at ~10^{-3} Torr) have accelerated OzID,[28] yet greater efficiency is desired.

Fundamentally, OzID is limited to the isomers with one unsaturated FA (uFA) on a defined site having DB(s) in alternative position(s), commonly counted from that site as Δn. The lipids with same uFA(s) on different sites (e.g., *sn*1 versus *sn*2 in the triacylglycerols, TG, or diacylglycerols, DG) or swapped uFAs (e.g., FAs with Δ6 on *sn*1 and Δ9 on *sn*2 versus the inverse) could not be distinguished *a priori*, like those with cis/trans DBs. Many FAs feature multiple DBs, wherein even the FA is not uniquely identifiable: e.g., the lipids including (i) a single FA with Δ6, Δ9 vs. two FAs with Δ6 in one and Δ9 in the other or (ii) one FA with Δ6, Δ9 and one with Δ3, Δ11 vs. one with Δ3, Δ6 and one with Δ9, Δ11. The patterns grow more complex for the isomeric mixtures prevalent in biological samples, where each fragment must be linked to the specific precursor. The CID/OzID option with slow OzID of the products of rapid CID helps in some, but not all instances.[29]

This situation calls for best isomer separation prior to the OzID step. That is hard to execute using dispersive linear IMS as the output transient ion packets are incompatible with slow OzID. The reverse order (IMS of OzID products) is useful,[30] but does not substitute for the intact lipid fractionation followed by structurally descriptive fragmentation. This aligns with the drive for top-down proteomic workflows, now incorporating IMS and then non-ergodic dissociation (commonly electron transfer dissociation, ETD).[31] Slow ETD process is likewise not easily coupled after linear IMS, but is after FAIMS that affords arbitrarily slow scans and steady filtering of targeted species.[31] The power of FAIMS/ETD hybrid has been illustrated in proteomics and epigenetics.[31,32] The recently developed lipid analyses by FAIMS/OzID were hampered by the above-mentioned constraints of resolution, sensitivity, and speed on both FAIMS and OzID sides, and further by their combination such as low ion utilization in FAIMS multiplied by poor OzID yield.[33]

A potential solution is the metal cationization, achieved in ESI using the corresponding salts.[34-40] Linear IMS can resolve lipid and peptide isomers better as the K^+ adducts than protonated ions. The FAIMS separation of lipid isomers broadly improved for the alkali metal and (more so) Ag or Cu adducts.[22,33] For example, the mean pairwise r for a set of four TG and three phosphatidylcholine isomers with varying DB positions and symmetries in the complexes with H^+/NH_4^+, K^+, Ag^+ and Cu^+ was 1.2, 2.8, 3.3, and 5.6 (respectively) despite similar E_C and thus R values.[33] This likely reflects the metal attachment to an electron-rich DB forcing the refolding of lipid around that (now charged) site, augmenting the influence of DB position on the ion geometry and thus IMS properties. Then multiply-charged transition metals ought to magnify this effect because of greater charge (and thus charge-induced dipole interactions with lipid atoms) and directional *d*-electron bonds. The higher z should elevate E_C as for peptides, where E_C for z = 1 - 3 overall scales with z to raise R as outlined above.[41] A better selectivity on top of greater R metrics can deliver impressive resolution gains.

Metalation of biomolecules (e.g., by Ag^+ for peptides[34] and Fe^{2+} for lipids)[40] can enhance the structural utility of CID. The OzID efficiency for K^+ complexes resembled that for the H^+/NH_4^+ baseline.[33] The Ag^+ adducts exhibited OzID only for the lipids with two or more DBs at lower yields.[33] Presumably Ag^+ protected the bound DB from O_3, although that did not explain a major drop of yield. The Cu^+ complexes surprisingly just added an O atom.[33] Complexes of 2+ or 3+ metal ions with organics have unique CID pathways[36-40] depending on the metal and particularly its 2nd or 3rd ionization energy (IE2 or IE3) that govern the minimum ligand number for charge retention (n_{min}) and reduction. However, no OzID of such adducts was probed.

Here we explore FAIMS/OzID of lipids cationized by exemplary 2+ and 3+ metals (Pb, Mg, Ni, La). We found the improved isomer resolution and dramatic intensification of OzID with many novel channels. These gains, alone and particularly in concert, create a major new capability for metabolomics.

Experimental Methods

We used the Sciex QTRAP 6500 triple quadrupole/trap instrument with the SelexION FAIMS option. The ESI source was at 5.5 kV. We collected the mass spectra by scanning Q1 or Q3 and picked the peaks of interest for FAIMS analyses with wide U_C ranges to encompass all the signal. The FAIMS stage with a bisinusoidal waveform of 3 MHz frequency was operated at the maximum U_D = 3.0 kV with N_2 carrier gas and high throttle gas setting for utmost resolution.[42] The cell temperature was set to "low" (~100 ºC) to minimize the charge reduction. All E_C values were deduced at the peak half-maxima.

The instrument was modified[43,44] to confine ions in the Q2 cell for ozonolysis with t_{Oz} = 0.001 - 50 s. The ~15:85 O_3/O_2 mix was produced by an O_3 generator (HC30, Ozone Solutions) from UHP O_2 supplied at 0.1 L/min and delivered to this cell via a PEEKsil restriction (i.d. 50 μm, 100 μm length),[44] yielding P_{O3} ~ 0.3 mTorr. The fragment detection is limited to m/z < 1000, although heavier precursors can be isolated. The OzID data were acquired at fixed E_C or during a FAIMS scan.

We covered nine lipids (L) with identical 18:1 FAs in each: five TGs (monoisotopic m = 884.8 Da) and four DGs (*sn*1/*sn*2 occupancy, m = 620.5 Da), Figure 1. These TGs (except Ps3) had been examined by FAIMS/OzID as 1+ ammoniated and metalated ions, making a benchmark for the impact of multiple charging.[33] We dissolved the standards (Avanti, Alabaster, AL) or their mixtures to ~10 μM in the ~1:4 methanol/chloroform, doped the nitrates of metals (M) in Figure 1 at ~100 μM, and infused the samples to the ESI emitter at 10 uL/min.

Figure 1. Studied lipids (color-coded) and metals with valence states and pertinent IE values (eV).

Class	Name and description	Label
TGs	Trivaccenin 18:1(11*E*)/18:1(11*E*)/18:1(11*E*)	**V3**
	Trielaidin 18:1(9*E*)/18:1(9*E*)/18:1(9*E*)	**E3**
	Triolein 18:1(9*Z*)/18:1(9*Z*)/18:1(9*Z*)	**O3**
	Tripetroselinin 18:1(6*Z*)/18:1(6*Z*)/18:1(6*Z*)	**Ps3**
	Tripetroselaidin 18:1(6*E*)/18:1(6*E*)/18:1(6*E*)	**Pd3**
DGs	Divaccenin 18:1(11*E*)/18:1(11*E*)/0	**V2**
	Dielaidin 18:1(9*E*)/18:1(9*E*)/0	**E2**
	Dipetroselinin 18:1(6*Z*)/18:1(6*Z*)/0	**Ps2**
	Dipetroselaidin 18:1(6*E*)/18:1(6*E*)/0	**Pd2**

Metal	Ag(I)	Cu(II)	Mg(II)	Pb(II)	Ni(II)	La(III)
IE	7.6	20.3	15.0	15.0	18.2	19.2

Triacylglycerols: TG 18:1/18:1/18:1 ($C_{57}H_{104}O_6$, mass 884.78 Da)

Trivaccenin

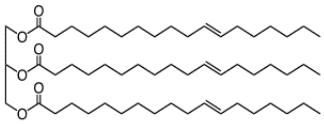

Trielaidin

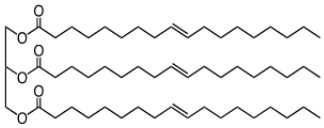

Triolein

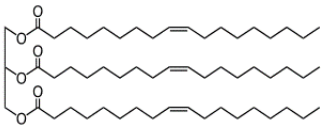

Tripetroselaidin

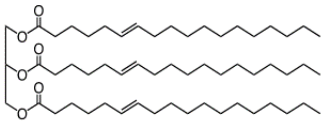

Tripetroselinin

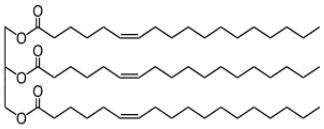

Diacylglycerols: DG 18:1/18:1/0 ($C_{39}H_{72}O_5$, mass 620.54 Da)

Divaccenin

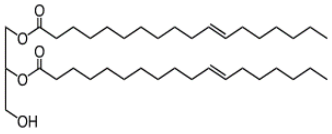

Dielaidin

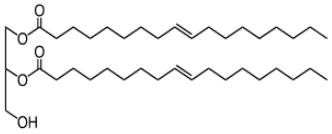

Dipetroselaidin

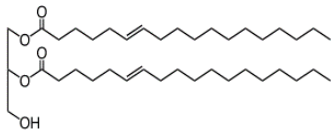

Dipetroselinin

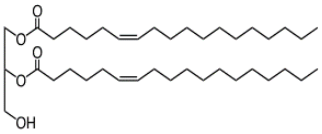

Results and Discussion

Triacylglycerols cationized by silver or copper

We first inspected the Ag/TG and Cu/TG complexes to compare with HD-FAIMS data.[33] The mass spectra for argentinated TGs show an intense M^+L envelope (Figures 2a, S1). A slightly bimodal E_C scan for the **V3**/**Ps3** mixture spreads over ~90 - 130 V/cm (Figure 2b). The same followed by OzID with t_{Oz} = 10 s exhibits the C and weaker A ions for **V3** and **Ps3**, Figure 2c. We also see non-specific CID products (M*, M*O) upon the FA loss (–282 Da) from ML and putative MLO. The scans for C and A ions from same precursor match, but lie at higher E_C for **Ps3** than **V3** fragments fitting the precursor scan for the mixture (Figure 2b). The E_C value for **Ps3** peak exceeds that for **V3** by 3.7%, close to the 5.0% increase from **V3** to **Pd3** in HD-FAIMS.[33] Those isomers were resolved well over baseline (r > 4) there but not materially (r < 0.2) here, though. The other TGs also coincide here, while in HD-FAIMS **O3** was fully resolved (r = 1.4 - 1.7) from co-eluting (r < 0.3) **V3** or **E3**. Present deterioration of resolution is due to much lower R ~ 4.5 here (Fig. 1b) vs. ~100 for HD-FAIMS:[33] separating the lipid isomers using the current setup shapes as a tall order.

We probed those complexes by OzID in detail by analyzing individual isomers over t_{Oz} = 4 - 50 s (Figure S2). The spectra are similar to Figure 2c, with high C/A intensity ratios tracking the data from ion trap. At longer t_{Oz}, the minor features from OzID of two FAs (CC, AC, AA) and sequential CID/OzID products (C*) verify the DB position (Figure S2k). The yields, defined as the intensity ratio of specified product to the precursor, are duly about linear with t_{Oz} (Figure 2d). Those at 8 s exceed the ion trap benchmarks at same t_{Oz} by ~10× (~10% vs. 1% for C ions). This reflects a commensurately higher P_{O3} in the

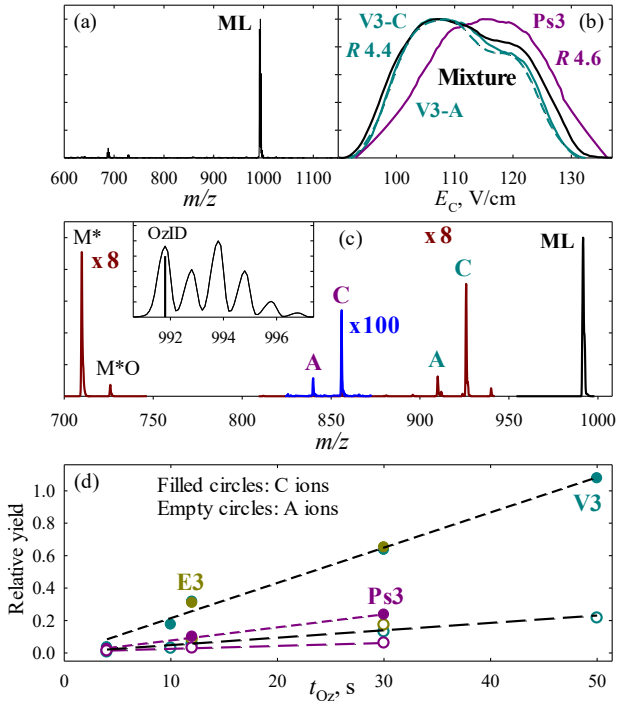

Figure 2. Normalized spectra for the Ag^+TG complexes: (a) MS of Ag^+/**V3** solution; (b) FAIMS for the **V3**, **Ps3** and their mixture extracted for C or A fragments (R values labeled); (c) FAIMS/OzID with the precursor MS window (inset), trace with magnified scale labeled, diagnostic fragments color-coded with C and A bolded. Panel (d) shows the yields of C and A ions versus the OzID dwell time with linear regressions.

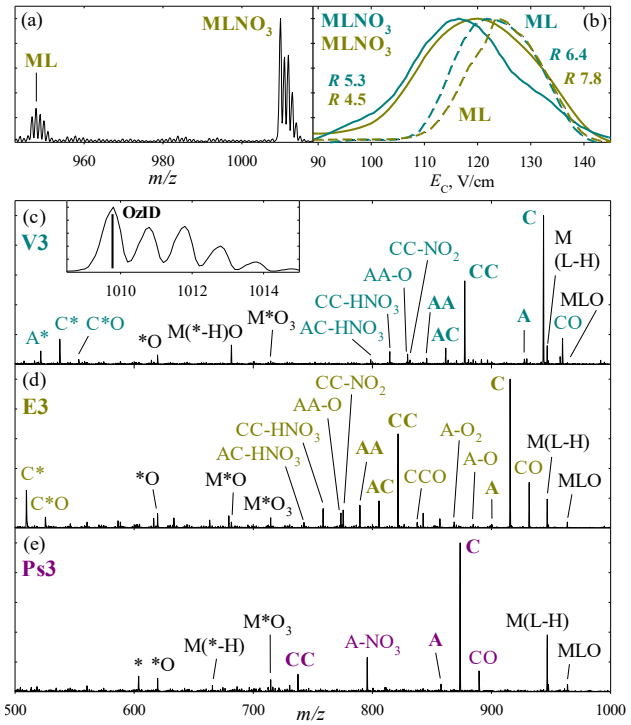

Figure 3. Spectra for the Cu/TG complexes: (a) MS of Cu^{2+}/**E3** solution; (b) FAIMS for M^+L (dash lines) and $[MLNO_3]^+$ (solid lines) with **V3** and **E3**; (c-e) OzID (t_{Oz} = 30 s) for $[MLNO_3]^+$ with **V3**, **E3**, **Ps3**. All ions are 1+, the nomenclature follows the Figure 2.

Q2 quadrupole, as reviewed above. The lower yields for **Ps3** complexes perhaps ensue from the steric hindrance to DBs closer to the ester moieties, as for the sphingosine FAs.[43]

The highest IE2 of divalent metals is for Cu, and the 2+ cuprated organic molecules are prone to charge reduction via dissociative proton or electron ($\bar{e}$) transfer.[36,37] Hence, doping by Cu(II) salts mostly yields the +1 ions in ESI. Here, the mass spectra are dominated by the Cu^+L/L^+ pair upon $\bar{e}$ transfer and $[Cu(L–H)]^+$ and $[CuLNO_3]^+$ with complementary H^+L upon H^+ transfer in the putative $Cu^{2+}L_2$ intermediates (Figures 3a, S3).

The Cu^+L species have slightly higher E_C and R values (R ~ 7) than the Ag^+ analogs (Figure 3b), per the known[14] anti-correlation between m and E_C for homologous species with m/z over ~500. The $[CuLNO_3]^+$ adducts accordingly have lower E_C and R values than Cu^+L, with peak broadening (R ~ 5) perhaps caused by convolution over multiple nitrate locations. For either, the **V3** and **E3** complexes completely merge (r ~ 0.1). The results for other TGs are similar. Again, in HD-FAIMS the Cu^+L with **V3**/**E3**, **O3**, and **Pd3** were resolved baseline but the **V3** and **E3** stayed merged.[33]

All Cu^+TG ions resisted OzID in earlier work[33] and do here even at t_{Oz} = 30 s despite the increase of $P_{O3}{\times}t_{Oz}$ factor controlling the yields by ~50× (Figure S4). Conversely, the $[CuLNO_3]^+$ species are amenable to OzID over t_{Oz} = 3 - 30 s (Figures 3 c - e, S5). The prominent C, A, CC, AC, and AA ions mirror those for Ag^+L. We also see the smaller diagnostic OzID fragments without $O/NO_2/HNO_3$ (e.g., AA – O, CC – NO_2, AC – HNO_3) and, per the reported Cu^+L oxidation, the MLO ion with OzID products (CO, CCO). The CID fragment M* is replaced by M^*O_2 and M^*O_3 (with all DBs oxidized) and non-metalated lipids minus FA (* and *O), with A* and C* likely from the ensuing OzID. Hence, the $[CuLNO_3]^+$ species seem more reactive than Ag^+L, although the precursor at m/z > 1,000 prevented quantifying that. Anyhow, the Cu^{2+} in $[CuLNO_3]^+$ cleaves the DB(s) much easier than the +1 Cu in Cu^+L.

Doubly-charged triacylglycerol complexes

Next we investigate the **V3** and **E3** (merged in HD-FAIMS)[33] with the dications of Mg and Pb having medium IE2 (Figure 1). We still see intense H^+ transfer leading to the H^+L and complementary $[MLNO_3]^+$ and $[M(L–H)]^+$ ions (for Mg only), Figure 4 a,c. Unlike with Cu complexes, no significant $\bar{e}$ transfer was encountered. The E_C scans for $[MgLNO_3]^+$ and $[Mg(L–H)]^+$ with **V3** and **E3** are all virtually identical (Figures 4b, S6) with E_C values just above those for Cu^+L and same R ~ 7 as anticipated. The peaks for $[PbLNO_3]^+$ with **V3** and **E3** are also identical with R ~ 7 and lie at somewhat lower E_C per the above mass correlation (Figure 4d). Hence, these TGs would not probably be resolved as 1+ ions with any metal.

The now substantial 2+ ions (Figure 4 a,c) come at much higher E_C: ~220 - 230 V/cm for $M^{2+}L_2$ and ~260 - 310 V/cm for $M^{2+}L$ (Figure 4 b,d). This order and greater values for Mg^{2+} than Pb^{2+} complexes are in line with said correlation, whereas the mean fwhm peak width (w) decreases from 17 V/cm for 1+ species to 10 V/cm for $M^{2+}L_2$ and 6 V/cm for $M^{2+}L$ - scaling roughly as $1/z$ per eq (1). The higher E_C and narrower peaks jointly raise R by up to six-fold, from 7 for 1+ to ~25 - 45 for 2+ ions. These large gains lead to a noticeable **V3**/**E3** separation, more so for Mg complexes with r = 0.6 for $Mg^{2+}L$. Even

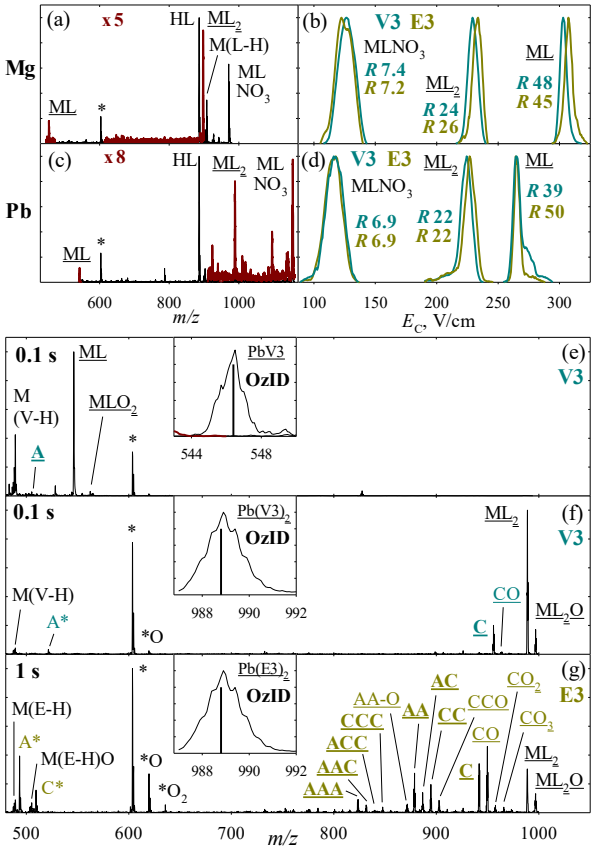

Figure 4. Normalized spectra for the Mg (a, b) and Pb (c - g) complexes with **V3** or **E3**: (a, c) MS of M^{2+}/**V3** solutions; (b, d) FAIMS for the $M^{2+}L$, $M^{2+}L_2$, $[MLNO_3]^+$ (R values labeled); (e-g) OzID (t_{Oz} = 0.1 or 1 s) for $Pb^{2+}L$ or $Pb^{2+}L_2$ (the precursor MS windows in insets). The traces with magnified scale are labeled, the 2+ ions are underlined, the diagnostic fragments are color-coded.

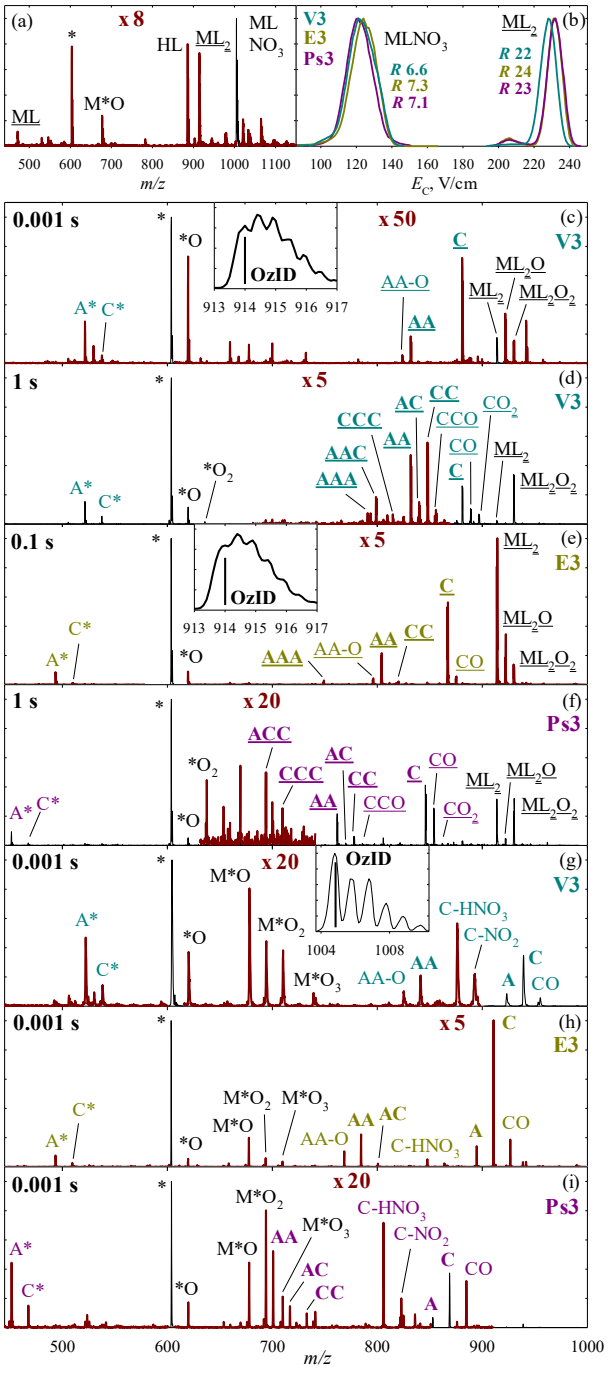

Figure 5. Spectra for the Ni complexes with **V3**, **E3**, or **Ps3**: (a) MS of Ni^{2+}/**V3** solution; (b) FAIMS for $M^{2+}L_2$ and $[MLNO_3]^+$; (c-f) OzID (t_{Oz} = 0.001 - 1 s) for $M^{2+}L_2$; (g -i) OzID (t_{Oz} = 0.001 s) for $[MLNO_3]^+$. The nomenclature follows the Figure 4.

this partial resolution exceeds that for 1+ Ag**V3**/Ag**E3** or Cu**V3**/Cu**E3** pairs in HD-FAIMS.[33]

We looked at the OzID of Pb^{2+} complexes (Figure 4 e-g). Already at t_{Oz} = 0.1 s, the 2+ oxides ($M^{2+}LO_2$, $M^{2+}L_2O$) and C and A ions are significant. The CID with charge splitting leading to * or *O is much stronger than for Cu complexes, and we now see the complementary $[M(FA–H)]^+$ with metal bound to departing FA. With t_{Oz} = 1 s (Figure 4g), we further get the 2+ products of OzID of two FAs (shadowing the 1+ ions for Ag or Cu complexes) and now all three FAs (CCC, ACC, AAC, AAA). The pathway to A is negligible for one OzID step but pronounced for two and especially three steps (note that all mixed A/C fragments are favored over pure ones by stoichiometry of 2:1 for AC and 3:1 for AAC and ACC). The C or CO ion yield reaching 0.2 in t_{Oz} = 0.1 s and 1.5 in 1 s (Figure 4 f,g) vs. respectively ~10 and >50 s in Figure 1d mean the OzID accelerated by ~100×. These findings for both FAIMS and OzID encourage assessing further polyvalent metals.

The metal dications can become more reactive with increasing IE2 and thus the energy benefit of charge transfer initiating many processes.[36] Thus we tried the divalent Ni with IE2 just below Cu (Figure 1). The mass spectra resemble those for Pb complexes (Figures 5a, S7). The E_C and R values in FAIMS scans for $[MLNO_3]^+$ and $M^{2+}L_2$ are also close (Figure 5b), again with no isomer separation for the former and barely any (r = 0.4 for **V3**/**E3**) for the latter. The OzID reactivity indeed goes up, with intense dioxide products ($M^{2+}L_2O_2$) and the C ion yield for **V3** or **E3** complexes increasing several times: to ~0.5 in 0.1 s and 10 (with precursor near-vanishing) in 1 s (Figure 5 c-f). As in Figure 2d, the yields for **Ps3** case are ~1/5 of those for **V3**/**E3**. Most importantly, the C fragment is readily observed (yield of 0.1) in the shortest feasible t_{Oz} = 1 ms (Figure 5c) and, based on the s/n ratio, would be detectable in yet shorter time.

As the fragment signal also scales with that of the precursor, of top practical interest is the OzID of most abundant ones - here $[NiLNO_3]^+$ with ~10× the intensity of $Ni^{2+}L_2$. Their products (Figure 5 g-i) track those for Cu analogs (Figure 3), with more intense 1+ metal oxide series up to M^*O_3 but the */*O CID fragments and their A* and C* derivatives as for Pb complexes. While the precursor m/z again precluded quantifying the yield, the signal and s/n ratio of C ion peaks for all isomers are outstanding already at t_{Oz} = 1 ms and (unlike in prior cases) longer times made little difference, Figure S8. This points to the OzID largely complete in 1 ms, essentially immediate for the analytical purposes. However, seeking the FAIMS separation of isomers, we advance to a trivalent metal.

Triacylglycerol complexes with lanthanum

As La has the lowest elemental IE3, the La^{3+} is least susceptible to charge reduction and makes 3+ adducts with various organic (including protic) molecules.[37,38] Unlike Mg, Pb, or Ni, La is effectively monoisotopic (^{139}La at 99.91%) which simplifies the MS analyses. Here we see the $M^{3+}L_n$ with n = 2 - 4 plus more intense lower-charged $[ML_nNO_3]^{2+}$ with n = 1, 2 and $[ML(NO_3)_2]^+$ complexes (Figures 6a, S9). The presence of trications (juxtaposed with the absence of dications for Cu) agrees with the charge reduction propensity regulated by relevant IE regardless of the charge state.[37]

In FAIMS, the $M^{3+}L_2$ complexes expectedly have yet greater E_C ~ 365 - 380 V/cm and R ~ 50 - 70 (some 10× that for 1+ analogs), Figure 6b. The now substantial isomer separations include baseline (r = 1.9) for **V3**/**Ps3** and close (r = 1.3) for **V3**/**E3**. The heavier $M^{3+}L_3$ species with suitably lower E_C ~ 300 V/cm and R ~ 40 - 50 still display same **V3**/**E3** resolution (r = 1.4), Figure 6c. The $[MLNO_3]^{2+}$ complexes have yet lower E_C ~ 250 - 290 V/cm and R ~ 40, Figure 6d. The w values (~6 V/cm) match those for the near-isobaric mono-ligand $Pb^{2+}L$: here the nitrate may latch to the +3 metal. The **V3** is separated baseline (r = 3.0 - 4.3) from all other isomers, and **Ps3** is well resolved (r ~ 1.3) from merged **E3**/**O3**. The heavier $[ML_2NO_3]^{2+}$ species with even lower E_C ~ 230 V/cm and R = 23 (similar to the bis-ligand $Pb^{2+}L_2$) show little **V3**/**E3** separation (r = 0.3), Figure 6e. The $[ML(NO_3)_2]^+$ peaks for those coincide

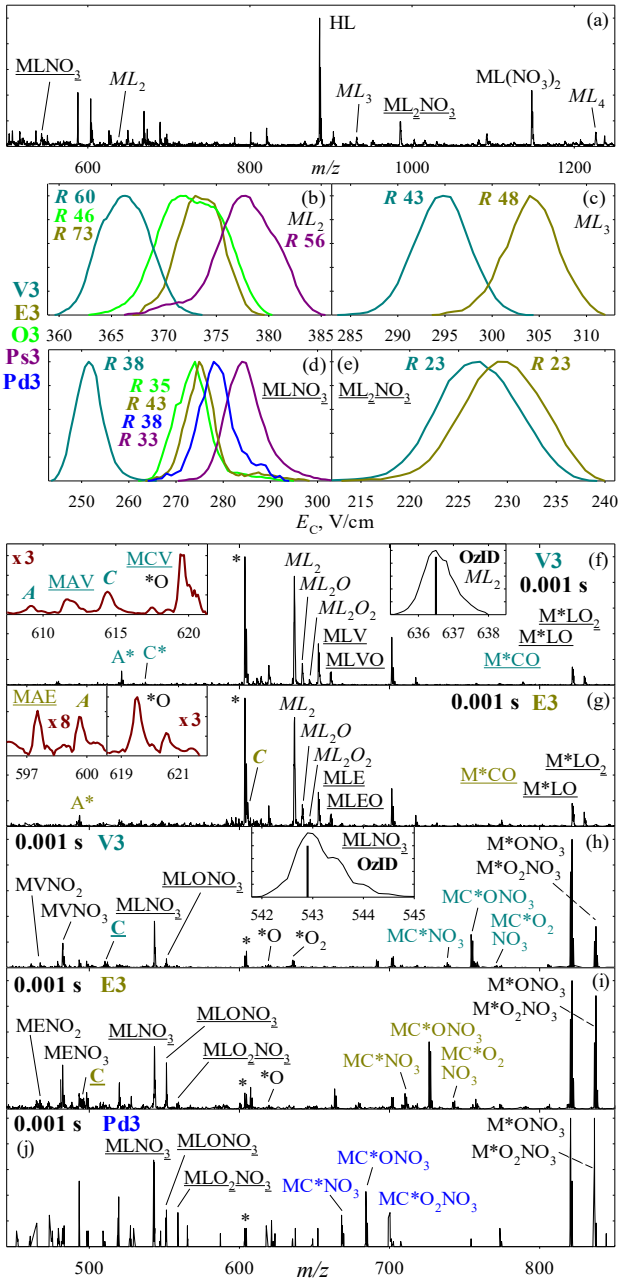

Figure 6. Normalized spectra for the La/TG complexes: (a) MS of La^{3+}/**V3** solution; (b-e) FAIMS for the 3+ (b,c) and 2+ (d,e) species (*R* values labeled); (f-j) OzID (t_{Oz} = 1 ms) for $M^{3+}L_2$ with **V3** and **E3** (f,g) and $[MLNO_3]^{2+}$ with **V3**, **E3**, and **Pd3** (h-j). The MS windows for OzID precursors and selected fragments are in the insets. The 3+ ions are in italic, the 2+ ions are underlined, the diagnostic fragments are color-coded.

at E_C ~ 120 V/cm with *R* ~ 7, mirroring the Ag and Cu complexes (Figure S10). Thus, the separations in Figure 6(b-d) stem primarily from multiple charging - not a peculiar La chemistry. The mean pairwise *r* values ($\bar{r}$) are 1.0 for $M^{3+}L_2$ and 2.0 for $[MLNO_3]^{2+}$ complexes: a wider separation space for the latter (13% vs. 3%) outweighs a lower *R* metric. The grand average of $\bar{r}$ = 1.6 is close to 1.4 for same TGs as ammoniated ions in HD-FAIMS: the gain from La^{3+} compares to the ~15× advantage in instrumental *R* and far exceeds it for the **V3**/**E3** pair.

The E_C values for $M^{3+}L_2$ and $[MLNO_3]^{2+}$ are linearly correlated with r^2 = 0.98 (Figure S11). Broadly, the E_C order of peaks in Figure 6d {**V3** < **O3** < **E3** < **Pd3** < **Ps3**} is retained over said La adducts and agrees with that for 2+ (Mg, Pb, Ni) and 1+ (Ag, Cu) complexes. This consistency over metals, compositions (one to three ligands and one or no nitrate), and charge states tells of a conserved structural facet within the lipids.

These TG isomer separations stand confirmed by the mixtures, Figure S12. However, the isomers can mix in multi-ligand adducts, e.g., M^{3+}**E3V3** and M^{3+}(**E3**)$_2$**V3** or M^{3+}**E3**(**V3**)$_2$. With no rigorous way to predict their E_C values, the above correlation suggests interpolating between the pure compounds. A strong signal between the **E3** and **V3** peaks for $M^{3+}L_2$ and $M^{3+}L_3$ but not $[MLNO_3]^{2+}$ supports this hypothesis and makes the mono-ligand adducts preferable from the practical perspective.

The OzID of $M^{3+}L_2$ in just 1 ms leads to 3+ mono- or di-oxides and C and A ion traces (Figure 6 f,g). Most products emerge from CID with charge reduction, including the dominant 1+ */*O with complementary 2+ ML(FA) and ML(FA)O, and 2+ M*LO and M*LO_2. The yield of diagnostic OzID fragments [the 2+ M*CO likely from M*LO and MC(FA)/MA(FA) from ML(FA), and the 1+ A* and C* ions] at ~0.1 compares to -that for Ni^{2+} complexes in same time. The $[MLNO_3]^{2+}$ species produce intense new 1+ CID fragments $M(FA)NO_3$ and the M*$O_{1,2}NO_3$ oxides with diagnostic OzID derivatives at higher yield of 0.5 - 1 in 1 ms (Figure 6 h-j). The bisligand $[ML_2NO_3]^{2+}$ behave like $Ni^{2+}L_2$ (Figure 5d), with CID into the intense */*O fragments and one or two slower OzID steps to 2+ C and A ions and their derivatives (Figure S13). This pattern permits disentangling the mixtures merged in FAIMS, as for Ag^+ complexes (Figure 2c). The synergy of good separation and "instant" OzID for $[MLNO_3]^{2+}$ is truly attractive. To assess its generality, we inspect the DG isomers.

Diacylglycerol complexes

The major argentinated ions are Ag^+L as for TGs, now with slightly greater E_C ~ 120 V/cm and *R* ~ 7 - 8 in FAIMS reflecting the lower mass (Figure 7a). As for TGs, the isomer resolution is nil with $\bar{r}$ = 0.1 and maximum *r* = 0.2 (for **E2**/**Pd2**).

The results for La complexes hugely differ. The MS spectra contain a small $M^{3+}L_n$ population as for TGs, with greater n_{min} = 3 sensible for smaller ligands (Figures 7b, S14). However, the 2+ ions are now the $M(L_n–H)$ mainly and ML_nNO_3 (both with *n* = 1 - 3), and the 1+ ions are M(L-H)NO_3 and $ML(NO_3)_2$ species. The above deprotonated 2+ and 1+ adducts arise from the dissociative H^+ transfer promoted by the protic OH group[38] found in DGs but not TGs. The complementary H^+L and its fragments upon loss of OH (*) and FA (**) are prominent.

The $M^{3+}L_3$ species appear at E_C ~ 360 - 380 V/cm, overlapping with the $M^{3+}(TG)_2$ at a similar mass (Figure 7c). With yet narrower peaks (*w* = 4 - 5 V/cm) and higher *R* ~ 70 - 80, all four isomers are separated well ($\bar{r}$ = 2.2) with the E_C order {**V2** < **E2** < **Ps2** < **Pd2**}. That ranking persists for $M^{3+}L_{4,5}$ but the metrics slide to E_C ~ 320 V/cm, *R* ~ 40 - 50, and $\bar{r}$ = 1.4 for *n* = 4 (similar to $M^{3+}(TG)_3$ close in mass) and then E_C ~ 270 V/cm, *R* ~ 30, and $\bar{r}$ = 1.1 for *n* = 5 (Figures 7d, S15a). This order holds for 2+ adducts, except **Ps2** and **Pd2** swapped in the mono-ligand M(L–H) and $MLNO_3$ species (Figures 7 e-h, S15b). The 2+ complexes have lower E_C ~ 200 - 300 V/cm and instrumental *R* ~ 20 - 40 as expected, tracking the $[M(TG)_{1,2}NO_3]^{2+}$ ions in same mass range (Figure 6d). The greater E_C for bis- than mono- ligand species reflects the tail of ion type transition from "A" (E_C < 0) to "C" (E_C > 0) with increasing *m*/*z* up to ~500 (in N_2),[41]

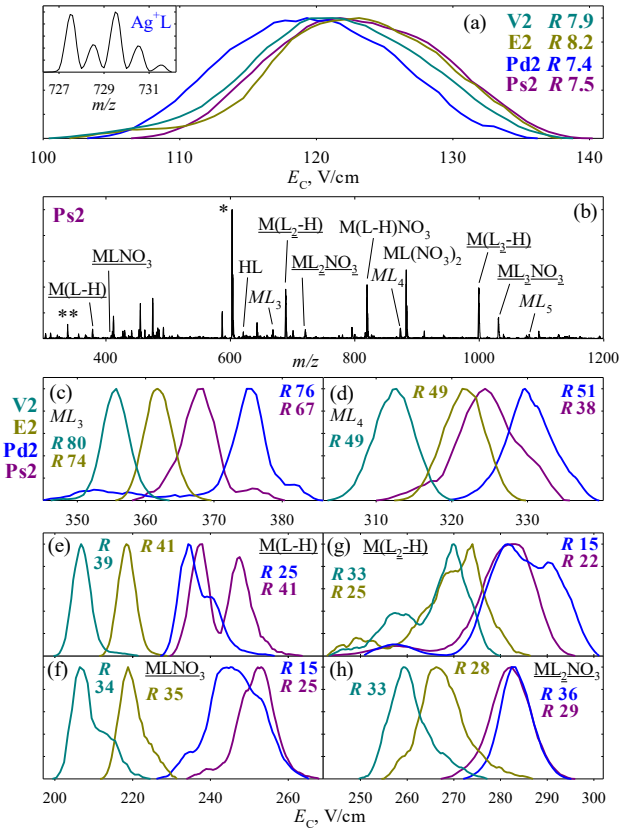

Figure 7. Spectra for the Ag/DG and La/DG complexes: (a) FAIMS for Ag^+L with MS window for **V3**; (b) MS of La^{3+}/**Ps2** solution; (c-h) FAIMS for selected 3+ and 2+ adducts. The nomenclature follows the Figure 6.

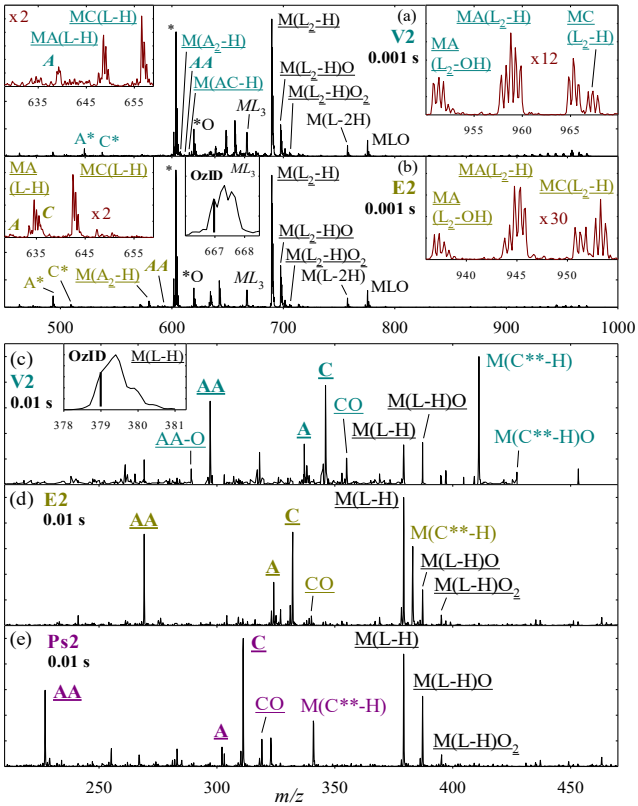

Figure 8. Normalized OzID spectra for La/DG complexes: (a, b) for $M^{3+}L_3$ with **V2** and **E2**; (c-e) $[M(L–H)]^{2+}$ with **V2**, **E2**, **Ps2**. The nomenclature follows the Figure 5.

and E_C decreases for $[ML_3NO_3]^{2+}$ at higher *m/z* values (Figure S15b). The two peaks for $[M(\mathbf{Ps2}–H)]^{2+}$ and major shoulders for $[M(\mathbf{Pd2}–H)]^{2+}$ and all $[M(L_2–H)]^{2+}$ and $[MLNO_3]^{2+}$ species indicate multiple geometries absent with the TGs. These may originate from La on the non-esterified OH at *sn3*. Nonetheless, the mono-ligand 2+ sets again have higher $\bar{\mathfrak{r}}$ (3.0 - 3.3) and maximum *r* (5.5) than the 3+ complexes because of wider separation space: 20 - 22% vs. 6%. That enables resolving all isomers (except **Pd2** from **Ps2**) baseline using the $[M(L–H)]^{2+}$ species, while $M^{3+}L_3$ or $[MLNO_3]^{2+}$ remain the choice for filtering **Pd2** from **Ps2**. The decrease of $\bar{\mathfrak{r}}$ with more ligands, to 1.7 for $[ML_2NO_3]^{2+}$ (Figure 7h) and 0.7 for $[ML_3NO_3]^{2+}$ (Figure S15b), tracks that for $M^{3+}L_n$ species. The $[ML(NO_3)_2]^+$ adducts have $R = 9$ and $\bar{\mathfrak{r}} = 0.4$ typical for 1+ ions (Figure S15c).

The eight 2+ and 3+ complexes (Figures 7 and S15 a,b) lend to 28 pairwise correlations between E_C of major peaks (Figure S16). The r^2 values are 0.69 - 0.99 with means and std. errors of 0.97 ± 0.013 in $z = 3$, 0.90 ± 0.025 in $z = 2$, an expectedly lower 0.84 ± 0.015 between $z = 2$ and 3, and 0.88 ± 0.015 overall. This evidences a structural facet across the ion compositions and charge states originating from the DG isomers, as with TGs. The E_C values for DG and TG complexes with identical FAs are also correlated, with same order **V** < **E** < **Pd**/**Ps** and r^2 of 0.75 for $[MLNO_3]^{2+}$ and 0.99 for $M^{3+}L_n$ species (Figure S17). Hence, that facet springs from the FA level. Such E_C increase with DB moving away from the chain terminus is noted for sphingosines[43] and may be general to lipids and FAs.

The DG isomer separations are also validated by isomeric mixtures, Figure S18. As with TGs, the traces for mono-ligand $[M(L–H)]^{2+}$ are superpositions of those for pure complexes but those for multi-ligand ones are not because of isomeric heterogeneity. With distant enough peaks for pure adducts, the mixed ones could be individually resolved rather than surmised from intense new bands. For example, the $M^{3+}L_3$ species from a 1:1 **V2**/**Ps2** mixture exhibit two peaks at ~2 - 4× the heights of those matching pure **V2** and **Ps2** complexes and splitting the E_C space between those into three equal segments. Again considering said linear correlation, we assign those as the $(\mathbf{V2})_2\mathbf{Ps2}$ and $\mathbf{V2}(\mathbf{Ps2})_2$ compositions with 3:1 stoichiometry to the pure complexes (assuming no isomeric binding bias). We can then attribute the intense broad distribution between the closer **V2** and **E2** complex peaks to merged $(\mathbf{V2})_2\mathbf{E2}$ and $\mathbf{V2}(\mathbf{E2})_2$ compositions.

The La/DG complexes also undergo ultrafast OzID, now with two maximum steps. The $M^{3+}L_3$ species yield modest 3+ C, A, and AA peaks, but (appropriately with protic ligands) the major channel is the dissociative H^+ transfer to $[M(L_2–H)]^{2+}$ and then $[M(L–2H)]^+$ (Figure 8 a,b). The former is oxidized in OzID and proceeds to more intense MC(L–H) or MA(L–H) with the yield of ~1 in 1 ms and then $M(A_2–H)$ species. The traces of parallel $MC(L_2–H)$ and $MA(L_2–H)$ with two intact lipids must come directly from OzID of $M^{3+}L_3$, revealing the possibility of charge-reducing OzID reactions. The 1+ CID/OzID products A* and C* are observed as usual. At longer t_{Oz} of 0.1 and 1 s, the precursor disappears while $[M(L_2–H)]^{2+}$ adds up to 5 oxygens and yields intense OzID products (Figure S19).

The mono-ligand $[M(L–H)]^{2+}$ complexes also exhibit fast OzID, with the 2+ oxide and intense A, C, CO, and AA ions (Figure 8 c-e). We also see intense new 1+ Criegee (but not aldehyde) ion M(C**–H) presumably from the OzID of M(**–H) intermediate from M(L–H) losing an FA. The yields of ~1 in 10

ms are similar to those for $M^{3+}L_3$ in 1 ms. The nitrated precursors yield A and C ions upon HNO_3 loss, with yields of ~1 in 1 ms (Figure S20). Hence, the conjunction of excellent separation and instant strong OzID for TG adducts was not an outlier.

Conclusions

We have extended FAIMS and OzID analyses to the lipids cationized by multiply-charged metal ions, namely the DGs and TGs with varying DB position or symmetry. The ESI of lipids mixed with proper salts has produced sundry 2+ and 3+ complexes with up to five lipid molecules or three lipids and the salt counter-ion (NO_3^-). As with peptides,[41] the FAIMS compensation field (E_C) increases by 2 - 3× over that for 1+ ions while the peaks narrow by 2 - 3× (approximately in proportion to the charge state z per the theory). Thus, the resolving power R goes up by ~5 - 10×: here from ~5 - 10 for benchmark 1+ ions (including H^+, NH_4^+, Ag^+, Cu^+) to ~20 - 50 for 2+ complexes (with Mg^{2+}, Pb^{2+}, Ni^{2+}, La^{3+}) and ~40 - 80 for 3+ La^{3+} adducts. This is by far the highest R recorded with the SelexION stage for lipids, although somewhat greater R were obtained for small molecules using vapors.[42] However, the divalent metals have not materially improved the isomer resolution of 1+ complexes - marginal if any with this system. The La complexes with both z = 3 and 2 (comprising NO_3^- or deprotonated lipid) furnish baseline separation of most DG and TG isomers. This gain can be rationalized by the highly-charged metal center attaching to the DB and rearranging the lipid geometry, thus modifying the IMS properties depending on the DB site. Whether this effect breaks out for La^{3+} solely on account of the 3+ formal charge or involves unique binding remains to be grasped.

While a greater gas pressure and thus O_3 partial pressure augments the OzID yield, this is available only in some IMS/MS platforms (e.g., Waters Synapt with cell at ~1 Torr). Thus, improving the intrinsic OzID efficiency remains worthwhile. The isomer-specific fragment/precursor quotient per dwell time jumps from ~0.01/s for Ag^+ to ~1/s for Pb^{2+}, ~10 - 100/s for Ni^{2+}, and ~100 - 1000/s for La^{3+} complexes with TGs or DGs. This acceleration by up to $\times 10^5$ (beyond that achieved by raising the O_3 pressure in any platform so far) likely comes from several factors including larger O_3 capture radius by the 2+ and especially 3+ ions and weakening of the C=C bonds by affixed metal polycations.

These gains upon multiple charging can be aggregated with known hardware improvements. That is, the R values in HDFAIMS should proportionately rise from ~100 for 1+ lipids to ~500 (the maximum demonstrated for multiply-charged peptides)[46] while OzID could be accelerated by another >100× as stated above. Present results further imply that (i) the transition metal cations may also improve the lipid isomer separation by linear IMS, where the instrumental R scales[47] as $z^{1/2}$ and the selectivity gains due to metal micro-solvation should also apply and (2) this mechanism may likewise improve the separations of other biomolecules including the peptides and glycans. Present OzID in ~1 ms could be inserted after dispersive linear IMS separations, especially in the SLIM[48] or multi-pass cyclic IMS[11] stages with eluting peak widths up to ~10 ms.

Supporting Information

Additional MS, OzID, and FAIMS spectra for further isomers and their mixtures under same or other conditions, and plots correlating the FAIMS separations across species.

ACKNOWLEDGMENT

This research was supported by NSF (CHE-1552640 and CHE-2105182) and Australian Research Council (DP190101486 and DP150101715). We thank Hayden Thurman and Dr. Bradley Schneider (Sciex) for the experimental and data processing help.

REFERENCES

1. H. Han, Q. *Lipidomics: Comprehensive Mass Spectrometry of Lipids.* Wiley (2016).
2. Hsu, F. F. *Mass Spectrometry-Based Lipidomics*. Humana Press (2021).
3. Holcapek, M.; Ekroos, K. *Mass Spectrometry for Lipidomics: Methods and Applications*. Wiley (2023).
4. Mitchell, T. W.; Pham, H.; Thomas, M. C.; Blanksby, S. J. *J. Chromatogr. B* **2009**, *877*, 2722.
5. Eiceman, G. A.; Karpas, Z.; Hill, H.H. *Ion Mobility Spectrometry* (3rd ed.). CRC Press, 2013.
6. Valentine, S. J.; Kulchania, M.; Srebalus Barnes, C. A.; Clemmer, D. E. *Int. J. Mass Spectrom*. **2001**, *212*, 97.
7. Shvartsburg, A. A.; Mashkevich, S. V.; Smith, R. D. *J. Phys. Chem. A.* **2006**, *110*, 2663.
8. Fenn, L. S.; Kliman, M.; Mahsut, A.; Zhao, S. R.; McLean, J. A. *Anal. Bional. Chem.* **2009**, *394*, 235.
9. Groessl, M.; Graf, S.; Knochenmuss, R. *Analyst* **2015**, *140*, 6904.
10. Jeanne Dit Fouque, K.; Ramirez, C. E.; Lewis, R. L.; Koelmel, J. P.; Garrett, T. J.; Yost, R. A.; Fernandez-Lima, F. *Anal. Chem.* **2019**, *91*, 5021.
11. Poad, B. L. J.; Jekimovs, L. J.; Young, R. S. E.; Wongsomboon, P.; Marshall, D. L.; Hansen, F. K. M.; Fulloon, T.; Pfrunder, M. C.; Dodgen, T.; Ritchie, M.; Wong, S. C. C.; Blanksby, S. J. *Anal. Chem.* **2023**, *95*, 15917.
12. Guevremont, R. *J. Chromatogr. A* **2004**, *1058*, 3.
13. Shvartsburg, A. A. *Differential Ion Mobility Spectrometry*. CRC Press (2008).
14. Shvartsburg, A. A.; Isaac, G.; Leveque, N.; Smith, R. D.; Metz, T. O. *J. Am. Soc. Mass Spectrom*. **2011**, *22*, 1146.
15. Berthias, F.; Baird, M. A.; Shvartsburg, A. A. *Anal. Chem.* **2021**, *93*, 4015.
16. Bowman, A. P.; Abzalimov, R. R.; Shvartsburg, A. A. *J. Am. Soc. Mass Spectrom.* **2017**, *28*, 1552.
17. Garabedian, A.; Baird, M. A.; Porter, J.; Jeanne Dit Fouque, K.; Shliaha, P. V.; Jensen, O. N.; Williams, T. D.; Fernandez-Lima, F.; Shvartsburg, A. A. *Anal. Chem.* **2018**, *90*, 2918.
18. Krylov, E. V.; Nazarov, E. G.: Miller, R. A. *Int. J. Mass Spectrom.* **2007**, 266, 76.
19. Shvartsburg, A. A.; Smith, R. D. *J. Am. Soc. Mass Spectrom.* **2007**, *18*, 1672.
20. Zhang, J. D.; Donor, M. T.; Rolland, A. D.; Leeming, M. G.; Wang, H.; Trevitt, A. J.; Kabir, K. M. M.; Prell, J. S.; Donald, W. A. *Int. J. Mass Spectrom.* **2020**, *457*, 116425.
21. Schneider, B. B.; Londry, F.; Nazarov, E. G.; Kang, Y.; Covey, T. R. *J. Am. Soc. Mass Spectrom.* **2017**, *28*, 2151.
22. Maccarone, A. T.; Duldig, J.; Mitchell, T. W.; Blanksby, S. J.; Duchoslav, E.; Campbell, J. L. *J. Lipid Res*. **2014**, *55*, 1668.
23. Sala, M.; Lisa, M.; Campbell, J. L.; Holčapek, M. *Rapid Commun. Mass Spectrom.* **2016**, *30*, 256.
24. Klein, D. R.; Brodbelt, J. S. *Anal. Chem*. **2017**, *89*, 1516.
25. Kirschbaum, C.; Pagel, K. *Analysis & Sensing* **2023**, *3*, e202200103.
26. Thomas, M. C.; Mitchell, T. W.; Harman, D. G.; Deeley, J. M.; Nealon, J. R.; Blanksby, S. J. *Anal. Chem.* **2008**, *80*, 303.
27. Vu, N.; Brown, J.; Giles, K.: Zhang, Q. *Rapid Commun. Mass Spectrom.* **2017**, *31*, 1415.
28. Poad, B. L. J.; Pham, H. T.; Thomas, M. C.; Nealon, J. R.; Campbell, J. L.; Mitchell, T. W.; Blanksby, S. J. *J. Am. Soc. Mass Spectrom.* **2010**, *21*, 1989.

29. Marshall, D. L.; Pham, H. T.; Bhujel, M.; Chin, J. S. R.; Yew, J. Y.; Mori, K.; Mitchell, T. W.; Blanksby, S. J. *Anal. Chem.* **2016**, *88*, 2685.
30. Poad, B. L. J.; Zheng, X.; Mitchell, T. W.; Smith, R. D.; Baker, E. S.; Blanksby, S. J. *Anal. Chem.* **2018**, *90*, 1292.
31. Baird, M. A.; Shliaha, P. V.; Anderson, G. A.; Moskovets, E.; Laiko, V.; Makarov, A. A.; Jensen, O. N.; Shvartsburg, A. A. *Anal. Chem*. **2019**, *91*, 6918.
32. Shliaha, P. V.; Gorshkov, V.; Kovalchuk, S. I.; Schwammle, V.; Baird, M. A.; Shvartsburg, A. A.; Jensen, O. N. *Anal. Chem*. **2020**, *92*, 2364.
33. Berthias, F.; Poad, B. L. J.; Thurman, H. A.; Bowman, A. P.; Blanksby, S. J.; Shvartsburg, A. A. *J. Am. Soc. Mass Spectrom.* **2021**, *32*, 2827.
34. Chu, I. K.; Guo, X.; Lau, T. C.; Siu, K. W. M. *Anal. Chem.* **1999**, *71*, 2364.
35. Zhu, F.; Glover, M. S.; Shi, H.; Trinidad, J. C.; Clemmer, D. E. *J. Am. Soc. Mass Spectrom*. **2015**, *26*, 25.
36. Shvartsburg, A. A.; Wilkes, J. G. *J. Phys. Chem. A* **2002**, *106*, 4543.
37. Shvartsburg, A. A. *Chem. Phys. Lett.* **2002**, *360*, 479.
38. Shvartsburg, A. A. *J. Am. Chem. Soc*. **2002**, *124*, 7910.
39. Shvartsburg, A. A.; Jones, R. C. *J. Am. Soc. Mass Spectrom.* **2004**, *15*, 406.
40. Becher, S.; Esch, P.; Heiles, S. *Anal. Chem*. **2018**, *90*, 11486.
41. Shvartsburg, A. A.; Prior, D. C.; Tang, K.; Smith, R. D. *Anal. Chem*. **2010**, *82*, 7649.
42. Schneider, B. B.; Nazarov, E. G.; Londry, F.; Vouros, P.; Covey, T. R. *Mass Spectrom. Rev*. **2016**, *35*, 687.
43. Poad, B. L. J.; Maccarone, A. T.; Yu, H.; Mitchell, T. W.; Saied, E. M.; Arenz, C.; Hornemann, T.; Bull, J. N.; Bieske, E. J.; Blanksby, S. J. *Anal. Chem*. **2018**, *90*, 5343.
44. Hancock, S. E.; Poad, B. L. J.; Willcox, M. D. P.; Blanksby, S. J.; Mitchell, T. W. *J. Lipid Res.* **2019**, *60*, P1968.
45. Shvartsburg, A. A.; Bryskiewicz, T.; Purves, R. W.; Tang, K.; Guevremont, R.; Smith, R. D. *J. Phys. Chem. B* **2006**, *110*, 21966.
46. Shvartsburg, A. A.; Seim, T. A.; Danielson, W. F.; Norheim, R.; Moore, R. J.; Anderson, G. A.; Smith, R. D. *J. Am. Soc. Mass Spectrom.* **2013**, *24*, 109.
47. Srebalus, C. A.; Li, J.; Marshall, W. S.; Clemmer, D. E. *Anal. Chem.* **1999**, *71*, 3918.
48. Deng, L.; Webb, I. K.; Garimella, S. V. B.; Hamid, A. M.; Zheng, X.; Norheim, R. V.; Prost, S. A.; Anderson, G. A.; Sandoval, J. A.; Baker, E. S.; Ibrahim, Y. M; Smith, R. D. *Anal. Chem.* **2017**, *89*, 4628.

ToC graphics